ACS Catalysis

Research Article

pubs.acs.org/acscatalysis

Density Functional Investigations of the Rh-Catalyzed Hydroformylation of 1,3-Butadiene with Bisphosphite Ligands

Sebastian Schmidt,[†] Peter Deglmann,[‡] and Peter Hofmann*[,†]

[†]Organisch-Chemisches Institut, University of Heidelberg, Im Neuenheimer Feld 270, D-69120 Heidelberg, Germany

[‡]BASF SE, GMC/M - G200, D-67056 Ludwigshafen, Germany

Supporting Information

ABSTRACT: The catalytic cycle of the Rh-catalyzed monohydroformylation of 1,3-butadiene with a triptycene-derived bisphosphite ligand was investigated with density functional theory, as it determines the selectivity of the 1,4-bis-hydroformylation of 1,3-butadiene to adipic aldehyde, a dream reaction of chemical industry. Out of the variety of possible reactive pathways, two dominant ones were highlighted leading to the monoaldehydes 3-pentenal and 4-pentenal, which experimentally also are the main primary products. With catalysts like the one studied here, which are highly *n*-selective and reactive for 1-alkene hydroformylation, 4-pentenal is known to be exclusively converted to the bis-hydroformylation product adipic aldehyde. An η^3-crotyl complex formed by *iso*-insertion of an (η^2-butadiene)Rh(H) species, not involved in hydroformylation reactions of 1-alkenes and requiring a slightly smaller activation barrier than the desired *n*-insertion, could be identified as an important intermediate for the monohydroformylation of butadiene. Once formed, this η^3-crotyl species opens up an unproductive exit channel within the catalytic reaction mechanism, which does not lead to adipic aldehyde. Free energy profiles in solution were calculated in order to find the intermediates and transition states that govern turnover frequency (TOF) and selectivity: The Rh crotyl complex and the reductive elimination transition state most likely limit the TOF, while the prediction of the regioselectivity is more complicated and depends on several steps.

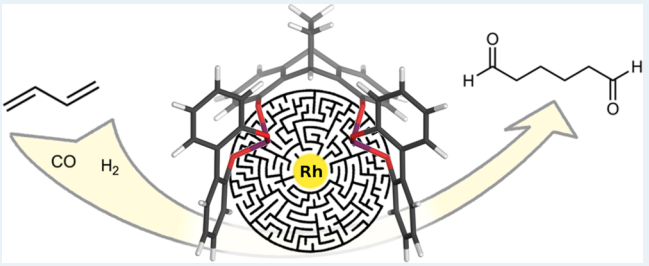

KEYWORDS: *hydroformylation, butadiene, adipic aldehyde, rhodium, DFT, reaction mechanism*

INTRODUCTION

Hydroformylation (the "oxo-reaction"), discovered by Roelen more than 75 years ago, is one of the largest homogeneous transition metal catalyzed processes in the chemical industry. Typically, nonconjugated terminal alkenes are transformed in an atom economic reaction with CO and H_2 to linear (*n*) or branched (*iso*) aldehydes, which subsequently can be converted to more desirable compounds like carboxylic acids, alcohols, and other important downstream products.[1] However, despite great success in finding highly *n*-regioselective catalysts for terminal alkenes, the bis-hydroformylation of conjugated dienes to linear dialdehydes, although a topic of much research since the 1950s, still remains highly problematic. Control of regio- and chemoselectivity are still major unsolved problems. In the case of the simplest diene, namely 1,3-butadiene, nowadays produced in steam cracker plants, more than a dozen different products can be formed and have been observed. Under typical reaction conditions, monohydroformylation (and hydrogenation) products, namely (*E*/*Z*)-3-pentenal and pentanal are formed as the main products.[2−7] It would be a promising commercial process, however, to selectively convert butadiene to 1,6-hexanedial (adipic aldehyde; eq 1), which is an attractive intermediate for the production of other valuable C6 compounds like adipic acid, hexamethylenediamine, and 1,6-hexanediol.[8−10]

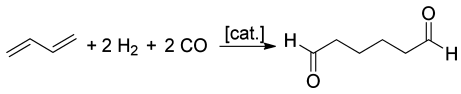

(1)

Of course, hydroformylation of butadiene has been investigated experimentally by many research groups during the past decades, but usually the selectivity for adipic aldehyde is low.[2−17] Recently, selectivities of up to 50% for adipic aldehyde could be obtained by our group with a new class of chelating bisphosphite ligands, congeners of the bisphosphine triptyphos (TTP, see below), which had been originally designed for high *n*-selectivities (up to *n*/iso ratios of over 300) **and** high turnover frequencies (above 1000 h^{-1}) in Rh-based hydroformylation catalysis of 1-alkenes (with only very minor amounts of isomerization and hydrogenation side reactions), as well as for hydrogenation and hydrocyanation (Ni) chemistry.[18−20] In the course of these studies of terminal mono-olefin hydroformylation, we also found that 4-pentenal, one of the possible regioisomers of butadiene monohydroformylation, is cleanly converted to adipic aldehyde (eq 2) using the same type of bisphosphite ligands.

Received: May 27, 2014
Revised: August 12, 2014
Published: September 3, 2014

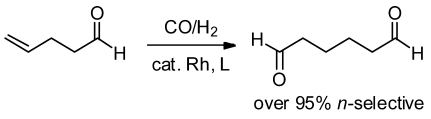

(2)

These results were the impetus to start looking at 1,3-butadiene hydroformylation. They add to our belief that it should be possible to further increase the selectivity for hexanedial by rational ligand design up to a level where a technical process becomes viable. However, the factors controlling the selectivity remain unclear, and a detailed study of the reaction mechanism with realistic phosphorus ligands is still missing. Without a basic knowledge about the reaction mechanism, successful ligand design is hard to achieve.

The mechanism of the hydroformylation of terminal mono-olefins has been studied extensively.[21] The commonly accepted mechanism was first proposed by Heck and Breslow[22] for unmodified cobalt catalysts and is analogous to the dissociative Wilkinson[23] mechanism for modified rhodium catalysts. It has been supported by many theoretical and experimental studies since then, although it must be said that not all the postulated single steps could be proven conclusively until now. The hydroformylation of conjugated dienes is much less understood. The second conjugated double bond alters the reaction behavior significantly and results in a number of additional possible reactive pathways for which experimental and theoretical information is scarce. One reason for the different behavior of conjugated dienes in contrast to terminal mono-olefins is the possibility to form η^3-crotyl complexes, which may initiate an isomerization of the remaining double bond and consequently result in a 1,4-addition of the hydrogen atom and the formyl group.[5,14,24−26]

Fell and co-workers[3,13] first observed dialdehydes and also small amounts of adipic aldehyde. They also studied the effect of different monophosphine ligands and reaction conditions on the product distribution and early on proposed a mechanism that can be used to explain the observed products (Scheme 1): The first hydroformylation takes place via either 1,2- or 1,4-addition. The 1,2-addition pathway is analogous to the hydroformylation of nonconjugated olefins and results mainly in 4-pentenal, which is subsequently hydroformylated like other terminal olefins (see eq 2). The 1,4-addition pathway proceeds via a crotyl complex and results mainly in 3-pentenal, which can react further in a second hydroformylation step of the internal double bond. Alternatively, 3-pentenal can undergo double bond isomerization to conjugated 2-pentenal, which is rapidly hydrogenated to pentanal under the reaction conditions. The latter pathway usually is preferred, thus pentanal is often found as the main product.

Van Leeuwen and Roobeek were able to obtain even 90% pentanal by employing a 1,2-bis(diphenylphosphino)ethane-Rh(I) catalyst and 5−20 bar syngas pressure.[4] They observed a very low reaction rate compared to the hydroformylation of mono-olefins in accordance with earlier findings[14] that hydroformylation does not take place at 1 bar syngas pressure. Their explanation for the low reaction rate was that the stable η^3-crotyl complex needs to undergo a hapticity change to an η^1-butenyl complex before insertion of CO can take place. However, their suggested mechanism mainly involves unsaturated 16 VE complexes and other species which one would regard as highly unstable from the present point of view.

Horiuchi et al. obtained 94% of 3-pentenal with the (*R*,*S*)-Binaphos ligand at 30 °C and 100 bar.[6] They explained the selectivities by a similar mechanism, but they left the detailed structure and ligand composition of the Rh-coordination sphere undefined.

Another explanation has been given by Ohgomori et al., who reported to have achieved 37% of adipic aldehyde with the DIOP ligand.[9] They suggested an equilibrium between axial−equatorial and equatorial−equatorial η^4-coordinated butadiene to be responsible for the selectivity between 1,2- and 1,4-addition, but without any conclusive experimental or theoretical evidence for this postulate.

Recently, Landis and Watkins, in an interesting study, explained the observed isomer distribution in asymmetric hydroformylation of substituted dienes with a $\pi-\sigma-\pi$ transformation in which the allyl ligand changes its coordination mode from η^3 to η^1 and back to η^3.[27]

Only very little basic mechanistic work has been done to verify any of the proposed mechanistic scenarios. Early reactivity studies showed that the addition of H−Co and H−Rh species to butadiene leads to the formation of η^3-crotyl complexes, which are relatively stable under hydroformylation conditions and facilitate 1,4-addition.[14,24,25] In situ HP-IR spectroscopic studies on unmodified cobalt and rhodium catalysts suggest the presence of η^3-allyl, η^1-butenyl, and acyl complexes as intermediates of the reaction.[28,29] Tuba et al.[30] confirmed the existence of an η^3-allyl intermediate in the Co-catalyzed hydromethoxycarbonylation of butadiene by IR and NMR spectroscopy; further investigation of the η^1-butenyl complex revealed its facile reaction to the acyl intermediate and the η^3-allyl type complex. Deuteroformylation experiments also indicated 1,4-addition of the deuterium atom and the deuterated formyl group.[5] Kinetic studies on the hydroformylation of isoprene and myrcene with Rh-bisphosphine

Scheme 1. Proposed Reaction Scheme for the Initial *n*- and *iso*-Insertion of 1,3-Butadiene into the Rh−H Bond and the Resulting Main Products of the Mono- and Bis-Hydroformylation

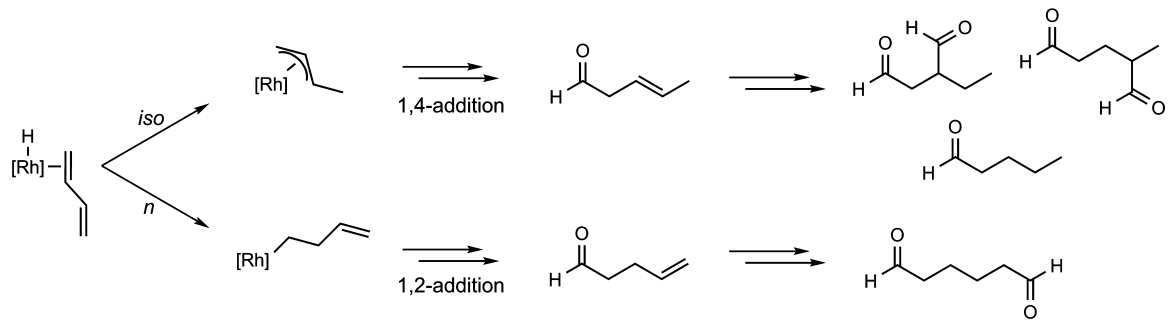

dx.doi.org/10.1021/cs500718v | ACS Catal. 2014, 4, 3593−3604

catalysts showed an increase of the reaction rate with increasing hydrogen and CO partial pressure, ligand concentration, and ligand basicity, but no dependence on the olefin concentration.[31] Thus, conjugated olefins show a completely different kinetic behavior compared to nonconjugated olefins, which supports the above statement that the allyl complex option significantly alters the reaction mechanism.

To the best of our knowledge, the only theoretical investigation of the full catalytic cycle of the hydroformylation of butadiene has been performed by Huo et al. employing an unmodified $HCo(CO)_3$ catalyst as their model system.[32] They investigated both linear and branched 1,2-addition pathways and the 1,4-addition pathway with DFT. The calculations showed a clear preference for the 1,4-addition pathway and an enhanced stability of the η^3-crotyl complex. Its formation has been classified as irreversible, and the CO-addition, which is accompanied by a hapticity change from η^3 to η^1, has been identified as the rate-determining step. These results are in line with the experimental findings described above. Yet still it is uncertain if the results can be transferred to rhodium catalysts with phosphine or phosphite monodentate or chelate ligands. Especially Gusevskaya's[31] finding that the rate of isoprene hydroformylation depends on the hydrogen partial pressure indicates that CO-addition is not the rate-determining step in this system. Moreover, noticeable amounts of adipic aldehyde could so far only be obtained with catalysts containing rhodium and chelating phosphorus ligands.

In the present study, the reaction mechanism of the Rh-catalyzed hydroformylation of 1,3-butadiene has been investigated theoretically using density functional theory employing one of our TTP-type bisphosphite ligands (Figure 1). The primary goal was to explain the observed product distribution and to gain further insight into the reaction mechanism in order to guide further experimental and theoretical studies directed toward a (semi)rational ligand design.

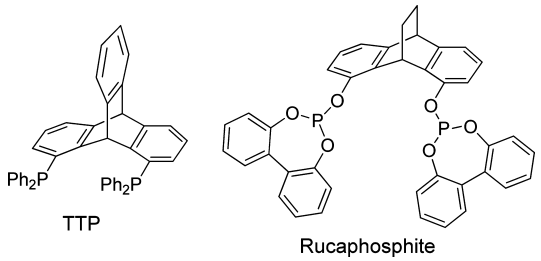

Figure 1. Triptyphos (TTP) and Rucaphosphite, a TTP-type bisphosphite ligand.

RESULTS AND DISCUSSION

Construction of Catalytic Cycles. For the investigation of the whole catalytic cycle, a total number of more than 700 stationary points, each with about 100 atoms, had to be examined. This required an approach that is feasible and still gives reliable results. We decided to use the GGA functional BP86[33] which already showed reasonable performance concerning structures and relative isomer energies for these types of complexes.[34] At each step of the catalytic cycle, a thorough manual screening of possible isomers was performed following a systematic scheme described in the Supporting Information. This approach does not cover the complete conformational space, but we are quite confident that we included the most relevant structures, e.g. *s-cis* and *s-trans* conformers of the butadiene and rotamers of the alkyl or acyl moieties. It is known that Rh(I) intermediates like the ones studied here are in a fast equilibrium with each other via rearrangement (e.g., Berry pseudorotation) or temporary CO coordination/decoordination.[35,36] Thus, for the energetics of the catalytic cycle, it is possible to focus on the most stable isomers (Curtin−Hammett principle).

To get an overview of the overall mechanism, we investigated several reaction pathways in analogy to the well-known sequence of elementary reaction steps in the dissociative Wilkinson mechanism: (a) olefin coordination to the active species of the catalyst, (b) olefin insertion into the metal−hydride bond, (c) CO insertion into the metal−alkyl bond, (d) oxidative addition of molecular hydrogen, and (e) reductive elimination of the aldehyde and regeneration of the active species. An overview of the intermediates and transition states which were investigated is given in Scheme 2, together with the free energies of the respective most stable isomer. In summary, there are three main pathways, called *n*, iso, and iso2, that lead to three different aldehydes, corresponding to the linear 1,2-addition product, the branched 1,2-addition product, and the 1,4-addition product, respectively. Each pathway splits into two subpathways, in which one of the coordination sites at the rhodium center is either occupied by CO or by the second C═C double bond. The latter is labeled with the suffix "−CO" (*minus* CO).

Relative Gibbs free energies of intermediates and transition states suggest that out of all these possibilities, two reactive pathways really matter in butadiene hydroformylation: One is a linear 1,2-addition pathway that leads to 4-pentenal and is analogous to the textbook reaction mechanisms for *n*-hydroformylation of 1-olefins. The other pathway leads to 3-pentenal in a formal 1,4-addition and involves isomerization *via* η^3-crotyl species after *iso* olefin insertion (hence "iso2"). The two relevant reaction cascades have been highlighted in Scheme 2 and will be discussed in detail in the next sections of this article.

The formed *n*-product 4-pentenal is known to react selectively to adipic aldehyde with our bisphosphite ligands.[19] 3-Pentenal can be further transformed to several products under the reaction conditions: Hydroformylation of the internal double bond leads to branched dialdehydes (2-ethylbutanedial and 2-methyl-pentanedial). Isomerization of the double bond can lead to the α,β-unsaturated aldehyde 2-pentenal, which is hydrogenated to pentanal under the reaction conditions. All expected aldehydes have been observed in our previous experimental studies.[19] The aldehydes resulting from the iso2 pathway are usually formed in larger amounts than 4-pentenal and adipic aldehyde, which is in accordance with our theoretical predictions that the iso2 pathway is favored (*vide infra*).

Free Energy Profiles. The two aforementioned pathways of n- and iso2-type are expected to account for the observed product formation due to their thermodynamic preference. We therefore performed more refined calculations regarding the total reaction rate and the *n*:*iso* selectivity for these two pathways. For this purpose, a more accurate free energy profile of the reaction is required. The main sources of inaccuracy of the BP86 profiles are (a) the inherent error of the BP86 exchange-correlation functional for reactions with transition metal complexes and its neglect of dispersive interactions, (b) the neglect of the vibrational partition function whenever translational and rotational degrees of freedom are converted to

dx.doi.org/10.1021/cs500718v | ACS Catal. 2014, 4, 3593−3604

Scheme 2. Intermediates and Transition States along the Possible Reaction Pathways of the Rh-Catalyzed Monohydroformylation of 1,3-Butadiene[a]

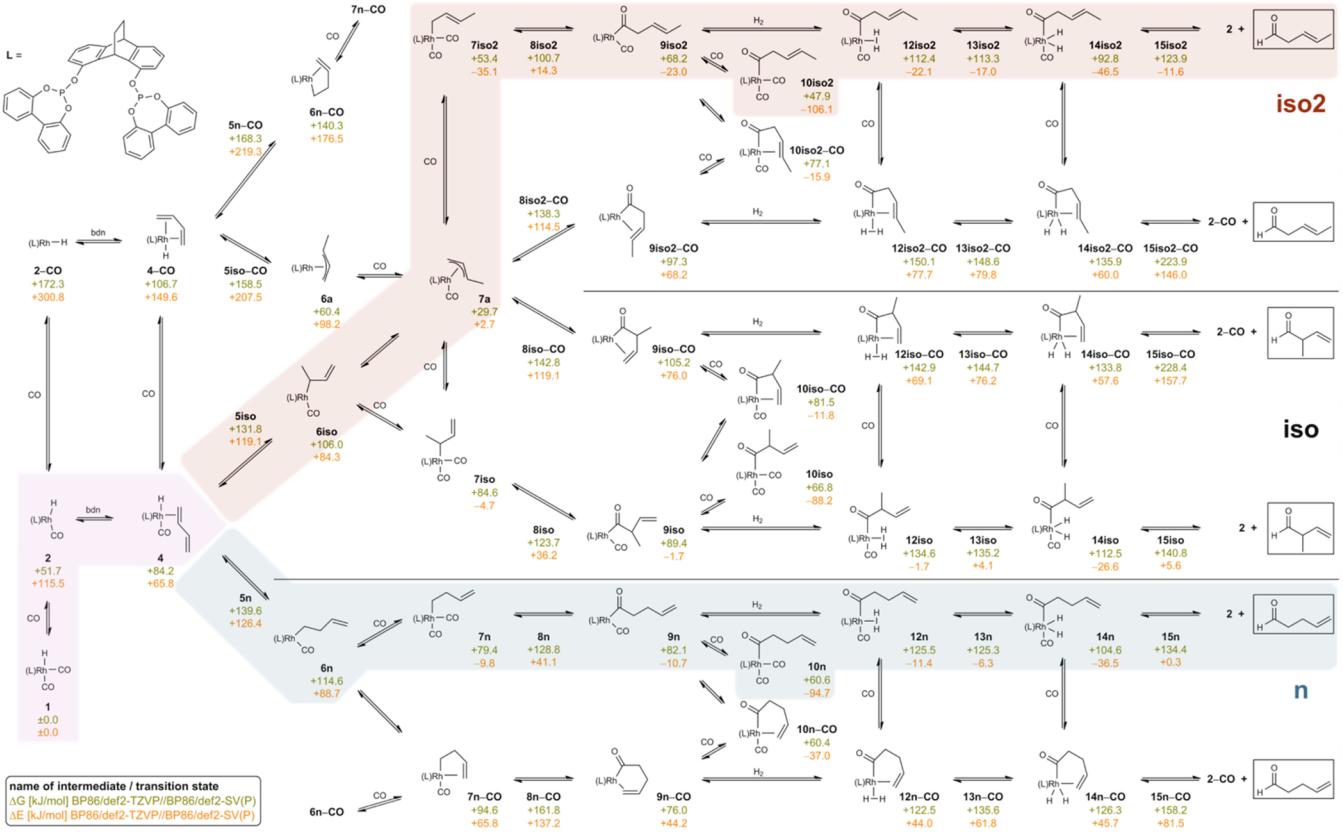

[a]Transition states for ligand coordination/dissociation, rearrangement, and isomerization pathways are not included here. The two thermodynamically preferred pathways to 4-pentenal and 3-pentenal are highlighted in color.

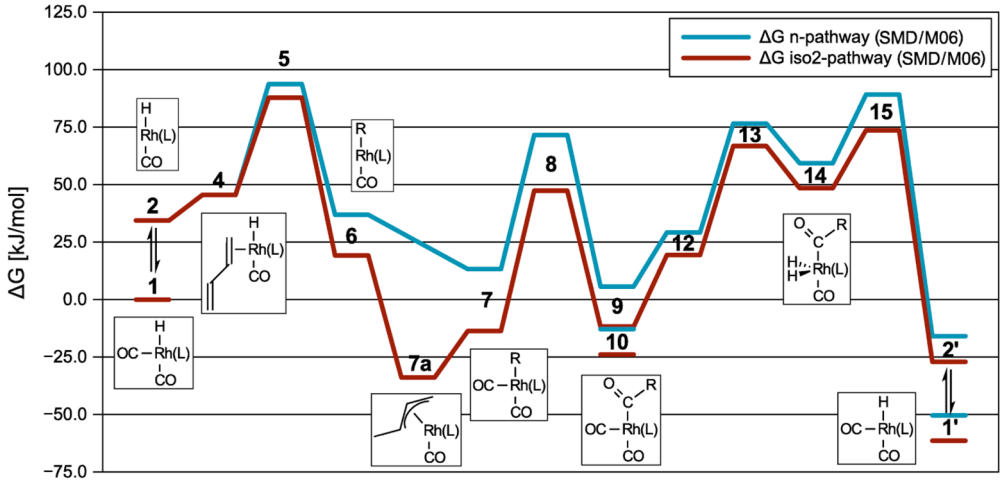

Figure 2. Free energy profiles of the *n* and iso2 pathways (SMD/M06/def2-TZVP//SMD/M06/def2-SV(P)). Barriers for isomerization and ligand coordination/decoordination processes are not included.

vibrations, *i.e.* during the ligand addition steps, and (c) the neglect of solvent effects. Removing these deficiencies alters the relative free energies of several steps in the catalytic cycle, especially the ligand addition processes. We thus recalculated (including structure relaxation) the most stable isomers of each step at the M06[37] level of theory, which represents a more accurate density functional, and applied the quasiharmonic approximation[38] for the vibrational partition function (raising all low modes to 100 cm^{-1} before using the usual harmonic oscillator approximation). We also included solvent effects for the model medium toluene with the SMD[39] solvation method in these calculations. Due to the increased computational demand, we could apply this method only to a selection of the most important structures. However, because of error cancellation for similar complexes, the BP86 calculations

dx.doi.org/10.1021/cs500718v | *ACS Catal.* 2014, 4, 3593−3604

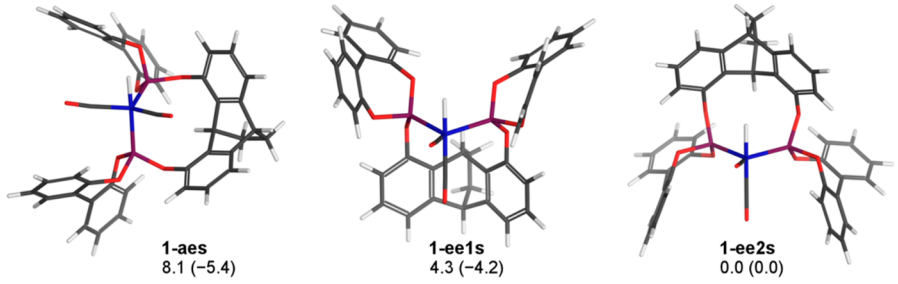

Figure 3. Structures of the most stable isomers of intermediate **1**: aes, ee1s, and ee2s. BP86 (SMD/M06) relative free energies in kJ mol^{-1} are given for each isomer.

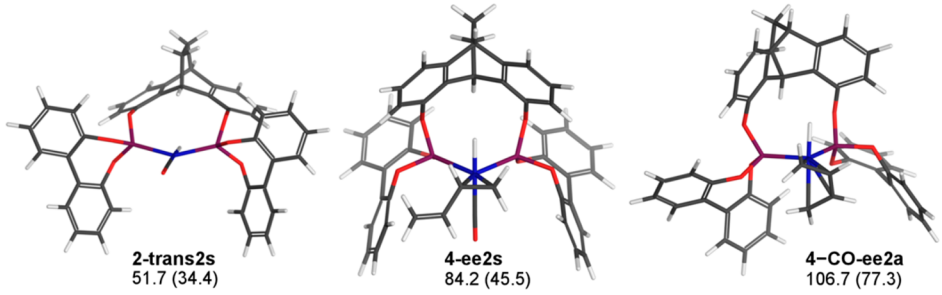

Figure 4. Structures of the most stable isomers of intermediates **2** and **4**. BP86 (SMD/M06) relative free energies in kJ mol^{-1} are given for each isomer.

should be reliable enough for the preselection within each stage of the catalytic cycle.

Altogether, most barriers were lowered significantly compared to BP86, which is more consistent with experimentally found reaction rates (from the data in ref 19, an activation barrier of roughly 100 kJ mol^{-1} can be estimated assuming a first order Eyring rate law). Additionally, several intermediates (**6**, **7a**, **7**, **9**, and **10**) were drastically lowered in free energy relative to the starting compound **1**. The resulting profiles are depicted in Figure 2. Barriers for isomerization and coordination/decoordination processes are not shown; however, it was established for several examples that these barriers are much lower in Gibbs free energy than the neighboring potentially rate-limiting transition states **5**, **8**, **13**, or **15**. Implications of these energy profiles for the kinetics and the selectivity of the reaction will be discussed in the last two sections of this article after the detailed discussion of the single steps.

Detailed Discussion of Intermediates and Transition States. In the following, important structural and energetic features of the rhodium species will be discussed step by step for all pathways in parallel. The findings will be compared to other works in this area. The discussion is based mostly on the BP86 free energies, since several isomers were taken into account. SMD/M06 free energies are also given where available.

*Hydrido Dicarbonyl Complex (**1**).* The hydrido dicarbonyl complex **1** is well-known as the preformed catalyst in the hydroformylation of mono-olefins. It is a saturated 18 VE species with a trigonal bipyramidal structure. The formally anionic hydride ligand has a strong preference to be in an axial position.[34,35,40] Thus, with our bisphosphite ligands, there are three possible isomers, one with the ligand in axial−equatorial (ae) position and two with equatorial−equatorial (ee) coordination and a different orientation of the ligand backbone (Figure 3). The three isomers **1-ee1s**, **1-ee2s**, and **1-aes** are similar in free energy with both BP86 and SMD/M06. We recently published the characterization of this complex with a slightly different ligand in solution and in the solid state.[34] In solution, an equilibrium between ae and ee coordination was found, which confirms that the energy difference between these two fluxional forms is very small.

The first step in the catalytic cycle is the generation of the active species **2** by dissociation of one CO ligand. This process means a movement uphill on the potential energy surface. However, no local maximum along the Rh-CO distance is encountered (of course, it could exhibit a small free energy barrier). The equatorial CO in the ee isomer dissociates most readily, resulting directly in the square planar *trans* isomer of **2**.

*Active Species (**2**).* The hydrido monocarbonyl complex **2** has a square planar structure in which the bidentate ligand can either occupy two *cis* or two *trans* coordination sites (Figure 4). Both isomers are almost equally high in free energy (54.2 and 51.7 kJ mol^{-1}, BP86). This reflects the flexible feature of our TTP-type bisphosphite ligands to stabilize bite angles between 90 and 180°.[34,41]

In the literature, a transition state (**3**) for the coordination of olefins to the active Rh species has been discussed.[42,43] However, we did not find any significant barrier for this process. For example, the coordination of butadiene to **2-trans2s** proceeds smoothly to **4-ee2s** with an energy barrier of only 10 kJ mol^{-1}. By applying *ab initio* molecular dynamics calculations, Gleich and Hutter calculated a barrier for ethylene coordination to a monophosphine rhodium complex of 35−40 kJ mol^{-1}, which results mainly from entropic contributions.[43] Even with this entropic penalty, the free energy of **3** is still well below the transition state of olefin insertion (**5**) and thus should not be rate-determining.

*Olefin Complex (**4**).* Butadiene can coordinate in either η^2 or η^4 fashion occupying one or two coordination sites in the trigonal bipyramid. It is known from η^2-bound mono-olefin complexes that the olefin is preferably in the equatorial plane

dx.doi.org/10.1021/cs500718v | *ACS Catal.* 2014, 4, 3593−3604

while the hydride ligand occupies the axial position.[40] This is also true in our case. The most stable isomer **4-ee2s** has butadiene coordinated like a simple monoolefin in the equatorial plane (Figure 4). The bisphosphite ligand occupies the remaining two equatorial coordination sites where it enhances π-back-bonding to the η^2-bound butadiene due to its σ-donor capabilities. We were also interested in the η^4-coordination mode, since it has been assumed as part of the suggested mechanisms in the literature.[4,9] With the hydride at the axial position of the trigonal bipyramid, butadiene can coordinate either equatorial−equatorial or axial−equatorial. Ohgomori et al. proposed the equilibrium between these two isomers to be responsible for the selectivity between the 1,2- and 1,4-addition pathways.[9] However, they did not have any evidence for this suggestion. Our calculations show that, in both isomers, the process of substituting one CO ligand in **4** with the second double bond of the butadiene (leading to **4−CO**) is clearly disfavored (by more than 20 kJ mol^{-1} in free energy at the BP86 level and 30 kJ mol^{-1} for SMD/M06). The same has been concluded for an unmodified cobalt catalyst.[32]

*Olefin Insertion (**5**).* The transition state for olefin insertion into the rhodium-hydride bond (which is better described as a hydride migration from Rh to the butadiene carbons C1 or C2) is a crucial point in the catalytic cycle. During this step, the connectivity of the final aldehyde products is determined. The insertion can take place either in an *n* or an *iso* fashion leading to *n*- or *iso*-alkenyl complexes, respectively. For both transition states **5n** and **5iso**, the coordinated butadiene needs to rotate out of the equatorial plane before hydride transfer can take place (Figure 5).

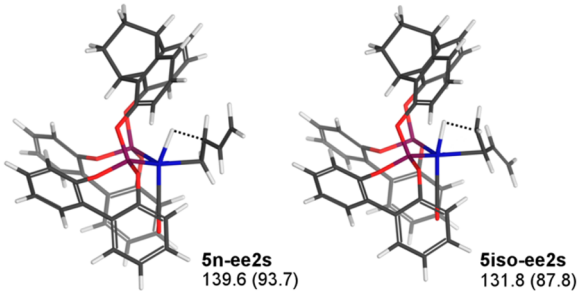

Figure 5. Structures of the most stable isomers of transition state **5**: *n* and *iso* insertion. BP86 (SMD/M06) relative free energies in kJ mol^{-1} are given for each isomer.

The most stable isomer in both cases is **ee2s**. The energy difference between *n* and *iso* is only a few kilojoules per mole, and the other isomers are also similar in energy (see Supporting Information). The preference for the *iso* insertion can be explained by the conjugated double bond, which stabilizes the transition state, similar to other conjugated substrates like styrene.[21] However, in this case the *n*−*iso* gap is small because from a steric point of view the highly *n*-selective TTP-type ligands would direct butadiene rather toward *n* insertion. Following the steepest-descent pathways for **5n-ee2s** and **5iso-ee2s** leads to **4-ee2s** and the agostic complexes **6n-cis2s** and **6iso-cis2s**, respectively.

Olefin insertion starting from the η^4-coordinated complex **5iso−CO** is about 30 kJ mol^{-1} higher in free energy (BP86) than the η^2 pathway with the additional CO ligand. In the case of the *n* insertion, the η^4 transition states are even more strained and thus are about 60 kJ mol^{-1} higher than the transition states with coordinated CO. Thus, olefin insertion is unlikely to proceed without the additional CO ligand, which disagrees with the proposed mechanisms of Ohgomori[9] and van Leeuwen[4] et al. Also, the following steps with the coordinated second C═C double bond are generally higher in free energy than the corresponding intermediates with the second double bond noncoordinated. Therefore, the "−CO" pathways are unlikely to be the preferred reaction pathways and will not be discussed any further.

*Alkenyl Monocarbonyl Complexes (**6**).* The alkenyl complex **6** (Figure 6) is a 16-electron complex. The geometry can be best described as distorted square planar where the CO ligand is bent out of the plane in order to increase the overlap with the occupied d_{z^2} orbital to enhance π-backbonding, similar to Rh(I) olefin complexes for which experimental structures are already known.[44] The bending of the CO out of the plane can also be understood as a distortion toward a trigonal bipyramidal geometry with a vacant coordination site in the equatorial plane. This coordination site can easily be occupied by other ligands like CO (leading to **7**) or by agostic interactions. Indeed, geometry optimizations of several conformers of **6** converged to agostic complexes which have a β-hydrogen close to the rhodium.

The energy difference between agostic and nonagostic complexes as expected is only a few kilojoules per mole. However, since agostic complexes are formed directly after olefin insertion and Huo et al.[32] found a relatively high barrier for breaking this agostic interaction in their unmodified cobalt system, we investigated this process for the isomers **6n-cis2s** and **6iso-cis2s**, which directly result from the lowest olefin insertion transition states. For the agostic complex **6n-cis2s**, we performed a relaxed coordinate scan during which the Rh−C_{agost} distance was increased. It revealed that this process proceeds with a very low barrier in potential energy and free energy. Afterward, the nonagostic complex can be stabilized by coordination of CO. The coordination is significantly exergonic and proceeds with a small energy barrier of about 10 kJ mol^{-1}.

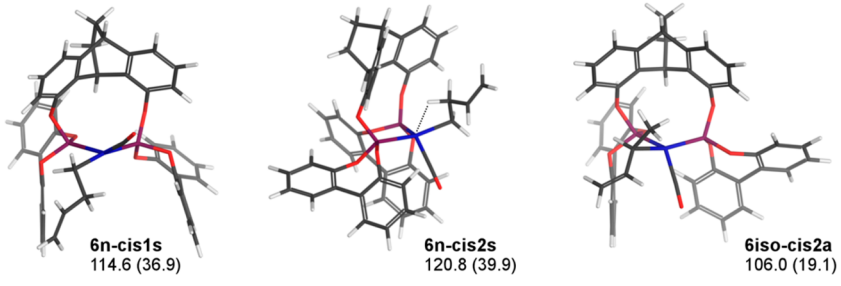

Figure 6. Structures of the most stable isomers of intermediate **6**. BP86 (SMD/M06) relative free energies in kJ mol^{-1} are given for each isomer.

dx.doi.org/10.1021/cs500718v | *ACS Catal.* 2014, 4, 3593−3604

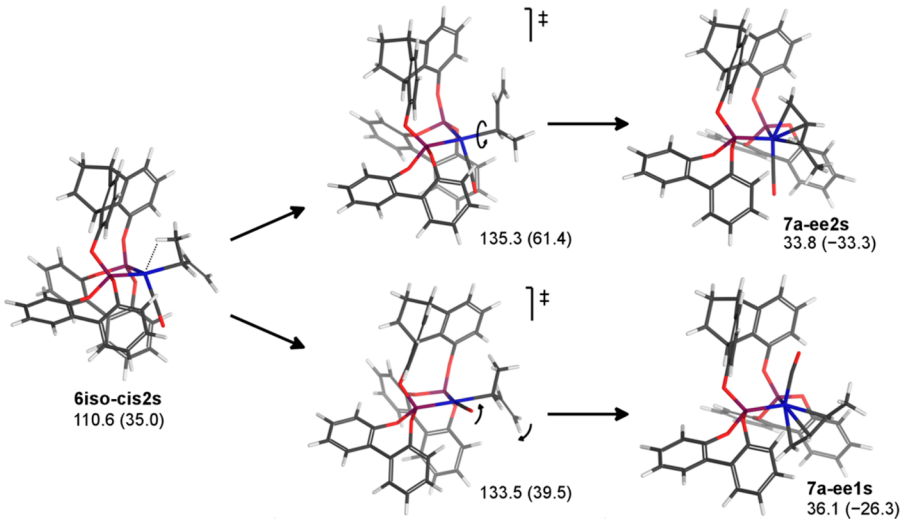

Figure 7. Rearrangement pathways of the alkenyl complex **6iso-cis2s** to the crotyl complex **7a**. BP86 (SMD/M06) relative free energies in kJ mol^{-1} are given for each structure.

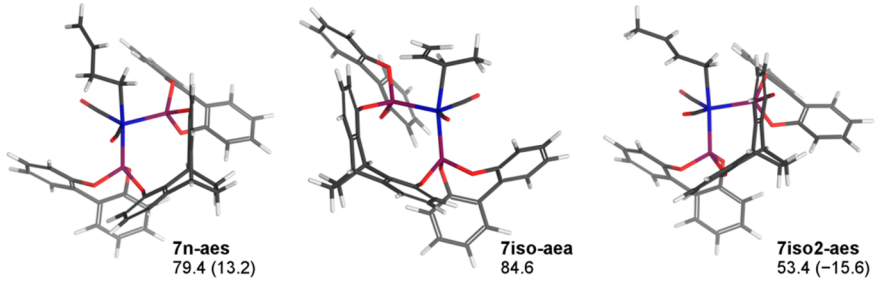

Figure 8. Structures of the most stable isomers of intermediate **7**. BP86 (SMD/M06) relative free energies in kJ mol^{-1} are given for each structure.

Thus, our calculations suggest that after *n* insertion the reaction proceeds rapidly to the alkenyl dicarbonyl complex **7n**. The agostic complex **6iso-cis2s** has been likewise investigated. The formation of **7iso** by CO addition proceeds just as in the case of **6n-cis2s**. Alternatively, it can rearrange to the η^3-allylic species **7a**. We found two low-lying transition states for this rearrangement leading to two different isomers of **7a**. Rotation around the Rh−C bond (Figure 7, top) leads to **7a-ee2s** and is about 25 kJ mol^{-1} (BP86) higher in free energy than **6iso-cis2s**. The second pathway involves a side change of the CO ligand via a square planar transition state (Figure 7, bottom) leading to **7a-ee1s** and is similarly high in free energy on the BP86 level. Both rearrangements are slightly higher in free energy than **5iso**, which suggests that formation of the crotyl complex is slower than the reverse reaction (β-hydride elimination) back to the butadiene complex **4**. Although many further—so far not considered—rearrangement reactions might slightly modify the picture, this finding suggests that reversibility of the insertion steps might be an important influence factor for the final product selectivity.

Alkenyl Dicarbonyl and Crotyl Complexes (7). The alkenyl dicarbonyl complexes **7n** and **7iso** are relatively stable, coordinatively saturated 18 electron complexes with a trigonal bipyramidal geometry and the alkenyl group at an axial position. The most stable isomers are **7n-aes** and **7iso-aea** (Figure 8), which result directly from CO addition to **6n-cis2s** and **6iso-cis2s**, respectively.

As mentioned before, the crotyl complex **7a** is thought to be the main reason for the different reaction behavior of dienes compared to nonconjugated olefins. It has a trigonal bipyramidal structure with the crotyl moiety bridging one axial and one equatorial position (Figure 7). The bisphosphite ligand occupies the remaining two equatorial positions. The most stable isomer is **7a-ee1a**, which has the CO ligand next to the ligand backbone and the methyl group of the crotyl moiety *syn* to the CO ligand. Compared to **7a-ee1s**, it differs only in the orientation of the biphenyl side groups. All isomers exhibit enhanced stability and are likely to be the resting state of the catalyst in accordance with previous interpretations that the crotyl complex reduces the reaction rate. CO addition to **7a** leads to either **7iso** or **7iso2**. Our calculations suggest a quasi-dissociative pathway via decoordination of the double bond with a CO nearby that supports this process and subsequently coordinates (Figure 9). The corresponding transition state lies

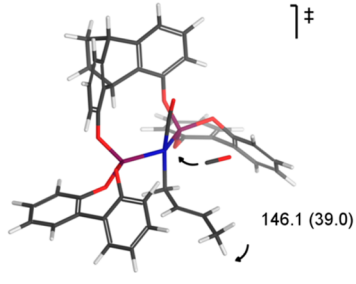

Figure 9. Transition state for the coordination of CO to the crotyl complex **7a-ee1s**, which leads to **7iso2-ee1s**. BP86 (SMD/M06) relative free energy is given in kJ mol^{-1}.

dx.doi.org/10.1021/cs500718v | *ACS Catal.* 2014, 4, 3593−3604

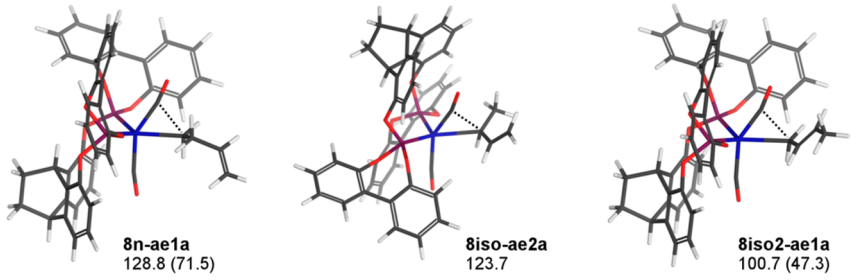

Figure 10. Structures of the most stable isomers of transition state **8**. BP86 (SMD/M06) relative free energies in kJ mol^{-1} are given for each structure.

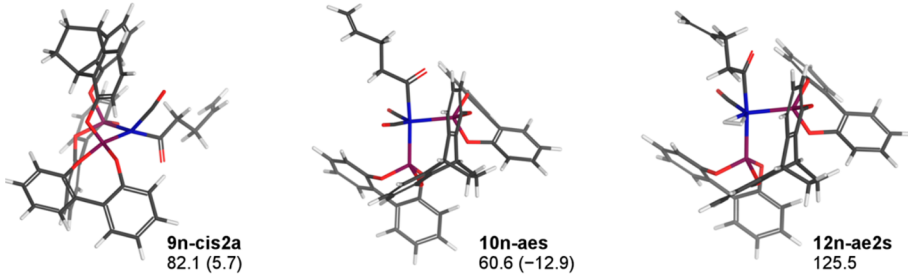

Figure 11. Structures of the most stable isomers of the intermediates **9**, **10**, and **12**. BP86 (SMD/M06) relative free energies in kJ mol^{-1} are given for each structure. The corresponding structures on the iso2 pathway look nearly the same, the only difference being the position of the remaining double bond.

quite high at the BP86 level (146.1 kJ mol^{-1}). Huo et al.[32] found a similar transition state for the unmodified cobalt system and concluded that it is the rate-determining step. However, recalculation at the M06 level plus solvation treatment yields a significantly lower barrier so that its relative free energy ends up well below the other transition states.

The dicarbonyl complex **7iso2** is similar to **7n** and **7iso**. Although **7iso2** and **7n** differ only with respect to the position of the remaining double bond, **7iso2** is 25−30 kJ mol^{-1} lower in energy. This is partly because of the more stable internal double bond and partly because of stabilization of the formal carbanion.

*CO Insertion (**8**).* The CO-insertion transition states (or more precisely, transition states for alkenyl migration to C_{CO}) of the three main pathways *n*, iso, and iso2 are quite similar to each other: The axial alkenyl group is bending toward one of the CO ligands where the new CO−alkenyl bond is formed while the Rh−alkenyl bond is broken. The lowest energy isomers are **8n-ae1a**, **8iso-ae2a**, and **8iso2-ae1a** (Figure 10). The corresponding conformers with a symmetrical orientation of the biphenyl side groups (**8n-ae1s**, **8iso-ae2s**, and **8iso2-ae1s**) are only marginally higher in energy.

8iso2 is considerably (23 kJ mol^{-1}, BP86) lower in energy than **8iso** because of the intrinsic stability of the alkenyl moieties, just like the rest of these two pathways. We thus omit further detailed discussion of the iso-pathway. Comparison of the two linear n and iso2 pathways is more important, because they yield the main products. The only difference between these pathways is the position of the remaining double bond. In **8iso2**, the double bond is still in conjugation with the migrating formal carbanion and thus stabilizes the transition state. In **8n**, the double bond is further away from the reactive center and does not have any significant effect. The steepest-descent paths for **8iso2-ae1s** and **8n-ae1s** lead to **7iso2-aes** and **7n-aes** and the agostic complexes **9iso2-trans1s** and **9n-trans1s**, respectively.

*Acyl Monocarbonyl Complexes (**9**).* Structural features of the acyl complexes **9** are similar to the alkenyl complexes **6**. They prefer distorted square planar geometries where the CO ligand deviates out of the plane. The most stable isomers are **9iso2-cis1s** and **9n-cis2a** (Figure 11).

After CO insertion, the remaining double bond is far away from the reaction center and the remaining parts of the n and iso2 pathways become very similar. Nevertheless, all iso2 isomers are about 10 kJ mol^{-1} lower in energy than their counterparts on the n pathway, which corresponds to the energy difference between a terminal and an internal double bond. Therefore, the iso2 pathway is intrinsically favored compared to the n pathway in the second half of the catalytic cycle.

According to Wilkinson's mechanism, there are two possible reaction pathways of the unsaturated acyl complex: temporary coordination of one additional CO to form the saturated acyl dicarbonyl complex **10** or the coordination and subsequent oxidative addition of a hydrogen molecule.

*Acyl Dicarbonyl Complexes (**10**).* The coordinatively saturated acyl dicarbonyl complex **10** has a trigonal bipyramidal geometry with the acyl ligand in an axial position. It represents a dead end in the catalytic cycle and could influence the reaction rate in the case of a too high stability. The most stable isomers are **10iso2-aes** and **10n-aes** (Figure 11). In order to proceed along the catalytic cycle, one CO ligand has to dissociate. This is, once again, a process without a significant reverse barrier on the potential energy surface.

*Dihydrogen Complexes (**12**).* The addition of H_2 (**11**) to the acyl monocarbonyl complex **9** forming the dihydrogen complex **12** is an endergonic reaction. We looked for possible transition states for the H_2 addition process (**11**) in the case of the two lowest isomers of **12**. We found that in these cases the easiest pathway is the addition of H_2 to the nonagostic acyl complexes **9** from the alkenyl side of the acyl group. This pathway has a small potential energy barrier due to some steric

dx.doi.org/10.1021/cs500718v | *ACS Catal.* 2014, 4, 3593−3604

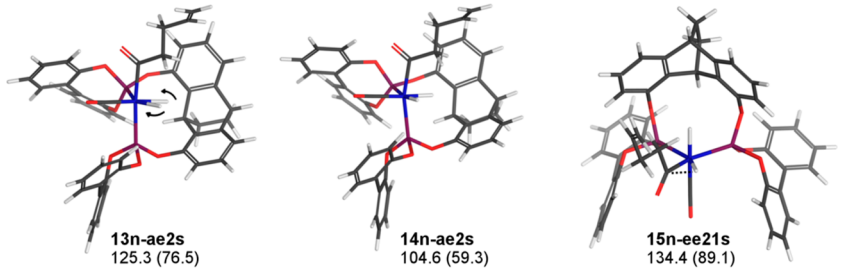

Figure 12. Structures of the most stable isomers of transition states **13** and **15** and intermediate **14**. BP86 (SMD/M06) relative free energies in kJ mol^{-1} are given for each structure. The corresponding structures on the iso2 pathway look nearly the same, the only difference being the position of the remaining double bond.

Scheme 3. Simplified Mechanistic Picture of the Mono Hydroformylation of Butadiene with Rh-Bisphosphite Complexes[a]

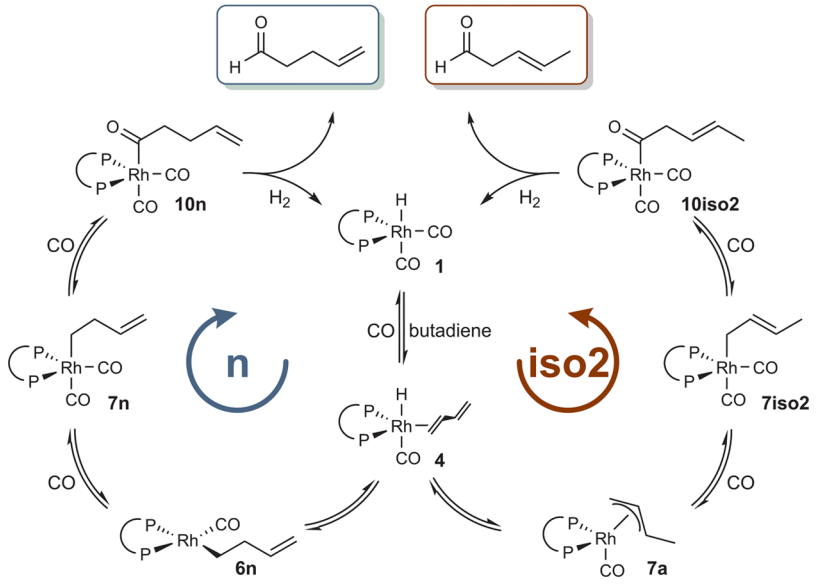

[a]Several reaction steps have been combined in order to give a concise overview.

hindrance of the acyl moiety. The relative free energies of the transition states are only about 10 kJ mol^{-1} higher in free energy than the resulting dihydrogen complexes **12**. These complexes have trigonal bipyramidal geometries with the acyl group in an axial position and the hydrogen in the equatorial plane (Figure 11). The bisphosphite ligand prefers axial−equatorial coordination. With SMD/M06, no local minima corresponding to σ-bound hydrogen could be located. Instead, van der Waals complexes with a Rh−H distance of 2.8 Å were obtained and are included in the energy profile of Figure 2.

*Oxidative Addition of H_2 (**13**).* The oxidative addition of H_2 proceeds readily in the dihydrogen complexes. The most stable isomers of this transition state are **13iso2-ae2s** and **13n-ae2s** (Figure 12), which directly follow the most stable isomers of **12** and lead to the most stable isomers of the dihydrido acyl complex **14**.

*Acyl Dihydrido Complex (**14**).* The last intermediate in the catalytic cycle is the acyl dihydrido species **14**. It is the only Rh(III) species in the cycle and the only one with an octahedral geometry. The three formally anionic acyl and hydrido ligands prefer *facial* coordination over *meridional* coordination because of the strong *trans* influences of these ligands. We define the acyl ligand to be at an axial position leaving again two possibilities for the bisphosphite ligand (ae and ee), of which the ae coordination is favored. The most stable isomers are **14iso2-ae2s** and **14n-ae2s** (Figure 12).

*Reductive Elimination (**15**).* Reductive elimination of the aldehyde is the last step in the catalytic cycle during which the active species of the catalyst (**2**) is regenerated and the unsaturated aldehyde is released. There are two different hydrogen atoms that can participate in the reductive elimination process. The hydrogen *trans* to the phosphite is predicted to be favored. The transition state has a pseudo-trigonal bipyramidal geometry with the aldehyde being eliminated in the equatorial plane and the remaining hydrogen in the axial position. The bisphosphite occupies the two remaining equatorial coordination sites. The most stable isomers are **15iso2-ee21s** and **15n-ee21s** (Figure 12). Calculations of the steepest-descent paths confirm that the elimination process starts from **14n-ae2s** and **14iso2-ae2s** and leads to **2-trans2s**. The free energy of this transition state is relatively high with 134.4 and 123.9 kJ mol^{-1} (BP86) or 89.1 and 73.6 kJ mol^{-1} (SMD/M06) for the n and iso2 pathways, respectively. Thus, within the uncertainty of the methods when comparing two different types of transition states, also reductive elimination could represent the rate-determining step (*vide infra*).

Summary of the Elementary Steps. The detailed and thorough study of all the proposed reaction pathways led us to

dx.doi.org/10.1021/cs500718v | *ACS Catal.* 2014, 4, 3593−3604

the conclusion that many of these can be disregarded in the further analysis of the reaction mechanism. We therefore propose a simplified mechanistic scheme, which is concise enough to provide a quick mechanistic overview, but still contains the most relevant information (Scheme 3). As already discussed in the previous sections, the two pathways n and iso2 are preferred in terms of free energy. The most noticeable difference compared to other hydroformylation reactions is the crotyl complex **7a**, which has a very high impact on the reaction behavior. Having identified the dominating pathways, we can now continue to discuss the kinetics and the selectivity of the reaction.

Rate-Determining Step and Order in Reactants. Some attempts have been made in the literature[29,31,32] to identify the rate-determining step of the hydroformylation of butadiene or of other dienes. For example, Huo et al. reported the CO addition to the crotyl complex as the rate-determining step because it has the highest barrier of all computed elementary reaction steps.[32] Under steady state conditions, however, the total reaction rate is governed by the highest effective barrier that has to be crossed during the whole catalytic cycle. This effective barrier can consist of one or more subsequent elementary reaction steps that connect the most stable reaction intermediate and the highest transition state. According to the SMD/M06 profiles (Figure 2), the two highest barriers connect the crotyl complex **7a** with the transition states for reductive elimination **15iso2** (107.5 kJ mol^{-1}) or H_2 addition **13iso2** (100.6 kJ mol^{-1}). Both possibilities are consistent with previous experimental observations, namely that conjugated dienes react significantly slower than nonconjugated olefins[14,29] and that the reaction rate for isoprene was found to be first order in CO and H_2 partial pressure but independent of olefin concentration.[31] Depending on the temperature and pressure, other barriers might also become rate-determining: **10iso2** to **15iso2** (97.5 kJ mol^{-1}), **10iso2** to **13iso2** (90.6 kJ mol^{-1}), and **1** to **5iso** (93.2 kJ mol^{-1}). In these cases, a different kinetic behavior would be expected.

On the n pathway, the most stable intermediates are **1** (−5.4 kJ mol^{-1}) and **10n** (−12.9 kJ mol^{-1}). The highest transition states are the olefin insertion **5n** (93.7 kJ mol^{-1}) and the reductive elimination **15n** (89.1 kJ mol^{-1}). It is likely that the turnover frequency of the n pathway is influenced partly by all of these states, resulting in a complex rate law. The energetic similarity of the transition states for reductive elimination and olefin insertion also suggests a partial reversibility of the n insertion.

Since the n-pathway closely resembles the main pathway of hydroformylation of terminal mono-olefins, a comparison with these reactions appears appropriate. The groups of Jensen and van Leeuwen found in theoretical investigations of the hydroformylation of ethene and 1-octene that the rate-determining step depends on the electronic properties of the ligand.[45] For electron-donating ligands like PPh_3, or a chelating bisphosphine with a similar backbone like the ligand used in this study, the olefin insertion step (the steps from **1** to **5n**) is rate-determining, whereas for less electron-donating ligands like phosphites, it is the hydrogenolysis step (the steps from **10n** to **15n**). Thus, a shift of the rate-determining step is observed when the electron-donor capability of the ligand is changed, which means that the difference between the two barriers is small. This is in agreement with our calculations and may mean that electron rich ligands exhibit different kinetics for the n pathway. However, this should not affect the overall kinetics of the hydroformylation of butadiene since the maximal energetic span for the n pathway is lower than for the iso2 pathway, which means that the overall reaction rate is determined by the iso2 pathway. This also means that under the considered reaction conditions the majority of the rhodium species should be present as **7a**, which acts as the resting state of the catalyst.

Prediction of Selectivities. The connectivity of the n and iso products is set during olefin insertion **5**. Thus, n:iso selectivity can be defined as the net flow through **5n** and **5iso**. If olefin insertion would be irreversible, n:iso ratios could be calculated from energy differences between **5n** and **5iso**. As discussed above, this difference is very small and could be responsible for the selectivities in the range of 20−50% found experimentally. However, it has been shown experimentally for similar systems that olefin insertion can be reversible.[46,47] Consequently, the n:iso ratio is additionally complicated by the degree of reversibility, which is much more difficult to predict than *n-iso* energy differences. Our calculations do not give a definite answer in this aspect, but several scenarios appear possible. Regarding the n-pathway, olefin insertion is predicted to be partly reversible because reductive elimination (**15n**) is almost equally high in free energy, and hence the forward reaction from the alkenyl complexes **6n** or **7n** may be slower than the backward reaction depending on the reaction conditions. The situation is different in the iso case. Once the allyl type complex **7a** is formed, the remaining transition states are predicted to be lower in free energy and thus the forward reaction should be faster than the backward reaction, rendering iso insertion irreversible. However, the barrier for rearrangement of the agostic alkenyl complex **6iso** to the crotyl complex **7a** may also cause some fraction of the alkenyl complexes formed to undergo β-hydride elimination back to the butadiene complex. On the BP86 level, this barrier is indeed high, but it is well below the transition state for olefin insertion with SMD/M06 (see Figure 6 and Supporting Information). In summary, prediction of the selectivity is not a straightforward task, and more than the two transition states **5n** and **5iso** have to be regarded. Moreover, the selectivity may strongly depend on the reaction conditions, especially temperature and pressure.

CONCLUSION

The catalytic cycle of the mono hydroformylation of butadiene with a TTP-type bisphosphite rhodium catalyst has been investigated with BP86 and SMD/M06 density functional theory. The additional conjugated double bond is the source of some important differences compared to the hydroformylation of terminal mono alkenes and alters the reaction mechanism. Some of the pathways discussed in the literature could be ruled out, and the main reaction pathways that lead to the experimentally observed product distribution have been identified.

The n pathway is very similar to the linear pathway in hydroformylation of terminal mono alkenes and leads to 4-pentenal, which (experimentally) is further converted to adipic aldehyde with TTP-type bisphosphite ligands. The iso2-pathway yields 3-pentenal and results from iso-insertion of butadiene into the Rh−H bond and subsequent double bond isomerization via an η^3-crotyl complex. The equivalent of the branched pathway in hydroformylation of terminal mono alkenes (iso pathway) is also possible but is higher in energy than the two competing n and iso2 pathways. Experimental selectivities are in agreement with our calculations. The formation of 3-pentenal is favored because of two reasons:

dx.doi.org/10.1021/cs500718v | ACS Catal. 2014, 4, 3593−3604

First, iso insertion is kinetically slightly favored compared to n insertion (about 5−10 kJ mol^{-1}). Second, the entire iso2 pathway is lower in energy than the n pathway because of the thermodynamically more stable internal double bond compared to the terminal double bond.

The crucial steps in the catalytic cycle for controlling the selectivity and the turnover frequency have been pointed out. The crotyl complex **7a** plays an important role as the most stable intermediate and is thus the reason why conjugated dienes react much slower in hydroformylation than monoolefins. Reductive elimination and oxidative addition of H_2 are most likely the rate-determining transition states. Regioselectivity is predicted to be controlled by a combination of several steps: olefin insertion **5n** and **5iso**, reductive elimination **15n**, and formation of the crotyl complex from the alkenyl complex **6iso**. Future ligand design should focus on these steps while keeping the general prerequisites of hydroformylation catalysts in mind.

Currently, experimental studies are going on in our lab, including mechanistic studies, *in situ* spectroscopy, Rh and Ir model complex chemistry, and high-throughput-screening of new ligands that have been rationally modified on the basis of our TTP-type bisphosphite ligands. The combined experimental and theoretical approach will guide further systematic developments in structural ligand variations, which will hopefully increase the selectivity for adipic aldehyde to a range well above 50% where a practical application becomes feasible.

COMPUTATIONAL DETAILS

All BP86 calculations were carried out with the program package TURBOMOLE 6.1.[48] Structures were fully optimized using the def2-SV(P) basis set[49] on all atoms together with a Stuttgart relativistic effective core potential[50] on Rh. Frequency calculations were carried out to identify the stationary points as true minima (zero imaginary frequencies) or transition states (one imaginary frequency) and to estimate the zero point vibrational energy (ZPE). IRC-like calculations were performed starting from the transition state and following the steepest descent path with a very small step size. Single point energies were calculated at the optimized geometries with the def2-TZVP[49] basis set. In all calculations with BP86, the RI approximation was used in order to speed up the calculation.[51] Gibbs free energy values (G) were calculated using standard statistic thermodynamics for rotational and translational degrees of freedom. The vibrational partition function, however, appeared to be very inaccurate because of very weak vibrational modes and was thus neglected.[52] All G values refer to our experimental conditions with 110 °C and 40 bar pressure.

Geometry optimizations and energy calculations of intermediates and transition states with M06[37] were carried out as described above using Gaussian 09[53] with the def2-SV(P) and def2-TZVP basis sets. The continuous solvent model SMD[39] was employed in these calculations with standard parameters for toluene, which is used in our experiments. During the calculation of the vibrational partition functions for the free energies, all low frequencies were raised to 100 cm^{-1} in order to avoid large errors caused by these low modes. Reference concentrations for all G values in solution are standard concentrations of 1 mol L^{-1} except for the gases which were presumed to be present in experimentally meaningful concentrations: CO, 0.2 mol L^{-1}; H_2, 0.05 mol L^{-1}.[54]

ASSOCIATED CONTENT

Supporting Information

Detailed description of the screening and nomenclature of the isomers. Absolute energies and relative free energies of all calculated structures. Relaxed coordinate scans for ligand dissociation processes. All computed molecule Cartesian coordinates in a format for convenient visualization. This material is available free of charge via the Internet at http://pubs.acs.org.

AUTHOR INFORMATION

Corresponding Author

*E-mail: ph@oci.uni-heidelberg.de.

Notes

The authors declare no competing financial interest.

ACKNOWLEDGMENTS

We thank the Fonds der Chemischen Industrie (PhD fellowship to S.S.) and the Deutsche Forschungsgemeinschaft (SFB 623, TP D4) for financial support of this work.

REFERENCES

(1) Weissermel, K.; Arpe, H.-J. *Industrial Organic Chemistry*, 4th ed.; Wiley-VCH: Weinheim, Germany, 2008; pp 127−144.
(2) Adkins, H.; Williams, J. L. R. *J. Org. Chem.* **1952**, *17*, 980−987.
(3) Fell, B.; Rupilius, W. *Tetrahedron Lett.* **1969**, 2721−2723.
(4) Roobeek, C. F.; van Leeuwen, P. W. N. M. *J. Mol. Catal.* **1985**, *31*, 345−353.
(5) Bertozzi, S.; Campigli, N.; Vitulli, G.; Lazzaroni, R.; Salvadori, P. *J. Organomet. Chem.* **1995**, *487*, 41−45.
(6) Horiuchi, T.; Ohta, T.; Shirakawa, E.; Nozaki, K.; Takaya, H. *Tetrahedron* **1997**, *53*, 7795−7804.
(7) Fell, B.; Hermanns, P.; Bahrmann, H. *J. Prakt. Chem.* **1998**, *340*, 459−467.
(8) Bunel, E. E. *Hydroformylation of conjugated dienes to alkenals using phosphonite ligands*. U.S. Patent 6,437,192, August 20, 2002.
(9) Ohgomori, Y.; Suzuki, N.; Sumitani, N. *J. Mol. Catal.* **1998**, *133*, 289−291 In this paper the authors unfortunately did not disclose all necessary details of their experiments, so that an exact reproduction of their work was not possible in our hands.
(10) Packett, D. L.; Briggs, J. R.; Bryant, D. R.; Phillips, A. G. *Process for producing 1,6-hexanedials and derivatives*. WO Patent 97/40003, October 30, 1997.
(11) Beati, E.; Natta, G. *Chimica e l'Industria (Milan)* **1945**, *27*, 84−87; *Chem. Abstr.* **1947**, *41*, 708.
(12) Brooks, R. E. *Process for the production of 5-carbon acyclic aldehydes*. U.S. Patent 2,517,383, Aug. 1, 1950.
(13) (a) Fell, B.; Boll, W. *Chem.-Ztg.* **1975**, *99*, 452−458. (b) Fell, B.; Boll, W.; Hagen, J. *Chem.-Ztg.* **1975**, *99*, 485−492. (c) Fell, B.; Bahrmann, H. *J. Mol. Catal.* **1977**, *2*, 211−218. (d) Fell, B.; Bahrmann, H. *J. Mol. Catal.* **1980**, *8*, 329−337.
(14) Brown, C. K.; Mowat, W.; Yagupsky, G.; Wilkinson, G. *J. Chem. Soc. A* **1971**, 850−859.
(15) Botteghi, C.; Branca, M.; Saba, A. *J. Organomet. Chem.* **1980**, *184*, C17−C19.
(16) van Leeuwen, P. W. N. M.; Roobeek, C. F. *A process for the hydroformylation of conjugated dienes*. Eur. Patent EP0033554A2, Jan. 12, 1981.
(17) Packett, D. L. *Hydroformylation process for producing 1,6-hexanedials*. U.S. Patent 5,312,996, May 17, 1994.
(18) Tauchert, M. E.; Warth, D. C. M.; Braun, S. M.; Gruber, I.; Ziesak, A.; Rominger, F.; Hofmann, P. *Organometallics* **2011**, *30*, 2790−2809.
(19) Smith, S. E.; Rosendahl, T.; Hofmann, P. *Organometallics* **2011**, *30*, 3643−3651.

(20) (a) Ahlers, W.; Röper, M.; Hofmann, P.; Warth, D. C. M.; Paciello, R. WO 01/58589, 2001. (b) Ahlers, W.; Paciello, R.; Röper, M.; Hofmann, P.; Tensfeldt, M.; Goethlich, A. WO 01/85739, 2001. (c) Ahlers, W.; Paciello, R.; Vogt, D.; Hofmann, P. WO 02/083695, 2002.
(21) For recent reviews see, e.g.: (a) Wiese, K.-D.; Obst, D. *Top. Organomet. Chem.* **2006**, *18*, 1−33. (b) van Leeuwen, P. W. N. M.; Claver, C. Rhodium Catalyzed Hydroformylation. In *Catalysis by Metal Complexes*; Kluwer Academic Publishers: Dordrecht, The Netherlands, 2002; Vol *22*, pp 1−144. (c) Torrent, M.; Sola, M.; Frenking, G. *Chem. Rev.* **2000**, *100*, 439−493.
(22) Heck, R. F.; Breslow, D. S. *J. Am. Chem. Soc.* **1961**, *83*, 4023−4027.
(23) Evans, D.; Osborn, J. A.; Wilkinson, G. *J. Chem. Soc. A* **1968**, 3133−3142.
(24) Husebye, S.; Jonassen, H. B.; Moore, D. W. *Acta Chimia Scandinavica* **1964**, *18*, 1581−1585.
(25) Heck, R. F.; Breslow, D. S. *J. Am. Chem. Soc.* **1961**, *83*, 1097−1102.
(26) Reilly, C. A.; Thyret, H. *J. Am. Chem. Soc.* **1967**, *89*, 5144−5149.
(27) Watkins, A. L.; Landis, C. R. *Org. Lett.* **2011**, *13*, 164−167.
(28) Mirbach, M. F. *Trans. Met. Chem.* **1984**, *9*, 465−468.
(29) Liu, G.; Garland, M. *J. Organomet. Chem.* **2000**, *608*, 76−85.
(30) Tuba, R.; Mika, L. T.; Bodor, A.; Pusztai, Z.; Toth, I.; Horvath, I. T. *Organometallics* **2003**, *22*, 1582−1584.
(31) (a) Barros, H. J. V.; Guimaraes, C. C.; dos Santos, E. N.; Gusevskaya, E. V. *Organometallics* **2007**, *26*, 2211−2218. (b) Barros, H. J. V.; da Silva, J. G.; Guimares, C. C.; dos Santos, E. N.; Gusevskaya, E. V. *Organometallics* **2008**, *27*, 4523−4531.
(32) Huo, C.-F.; Li, Y.-W.; Beller, M.; Jiao, H. *Organometallics* **2005**, *24*, 3634−3643.
(33) (a) Becke, A. D. *Phys. Rev. A* **1988**, *38*, 3098−3100. (b) Perdew, J. P. *Phys. Rev. B* **1986**, *33*, 8822−8824. (c) Perdew, J. P. *Phys. Rev. B* **1986**, *34*, 7406.
(34) Schmidt, S.; Abkai, G.; Rosendahl, T.; Rominger, F.; Hofmann, P. *Organometallics* **2013**, *32*, 1044−1052.
(35) Koga, N.; Jin, S. Q.; Morokuma, K. *J. Am. Chem. Soc.* **1988**, *110*, 3417−3425.
(36) Matsubara, T.; Koga, N.; Ding, Y.; Musaev, D. G.; Morokuma, K. *Organometallics* **1997**, *16*, 1065−1078.
(37) Zhao, Y.; Truhlar, D. G. *Theor. Chem. Acc.* **2008**, *120*, 215−241.
(38) Ribeiro, R. F.; Marenich, A. V.; Cramer, C. J.; Truhlar, D. G. *J. Phys. Chem. B* **2011**, *115*, 14556−14562.
(39) Marenich, A. V.; Cramer, C. J.; Truhlar, D. G. *J. Phys. Chem. B* **2009**, *113*, 6378−6396.
(40) Rossi, A. R.; Hoffmann, R. *Inorg. Chem.* **1975**, *14*, 365−374.
(41) (a) Rosendahl, T. Dissertation, University of Heidelberg, Germany, 2007. (b) Further structures of model complexes for butadiene hydroformylation and other reactions will be published separately.
(42) Landis, C. R.; Uddin, J. *J. Chem. Soc., Dalton Trans.* **2002**, 729−742.
(43) Gleich, D.; Hutter, J. *Chem.—Eur. J.* **2004**, *10*, 2435−2444.
(44) Urtel, H.; Meier, C.; Rominger, F.; Hofmann, P. *Organometallics* **2010**, *29*, 5496−5503.
(45) (a) Sparta, M.; Børve, K. J.; Jensen, V. R. *J. Am. Chem. Soc.* **2007**, *129*, 8487−8499. (b) Zuidema, E.; Escorihuela, L.; Eichelsheim, T.; Carbó, J. J.; Bo, C.; Kamer, P. C. J.; van Leeuwen, P. W. N. M. *Chem.—Eur. J.* **2008**, *14*, 1843−1853.
(46) Watkins, A. L.; Landis, C. R. *J. Am. Chem. Soc.* **2010**, *132*, 10306−10317.
(47) van der Slot, S. C.; Duran, J.; Luten, J.; Kamer, P. C. J.; van Leeuwen, P. W. N. M. *Organometallics* **2002**, *21*, 3873−3883.
(48) (a) Ahlrichs, R.; Bär, M.; Häser, M.; Horn, H.; Kölmel, C. *Chem. Phys. Lett.* **1989**, *162*, 165−169. (b) Häser, M.; Ahlrichs, R. *J. Comput. Chem.* **1989**, *10*, 104−111. (c) Treutler, O.; Ahlrichs, R. *J. Chem. Phys.* **1995**, *102*, 346−354. (d) von Arnim, M.; Ahlrichs, R. *J. Chem. Phys.* **1999**, *111*, 9183−9190. (e) Deglmann, P.; Furche, F.; Ahlrichs, R. *Chem. Phys. Lett.* **2002**, *362*, 511−518. (f) Deglmann, P.; Furche, F. *J. Chem. Phys.* **2002**, *117*, 9535−9338.
(49) Weigend, F.; Ahlrichs, R. *Phys. Chem. Chem. Phys.* **2005**, *7*, 3297−3305.
(50) Andrae, D.; Häußermann, U.; Dolg, M.; Stoll, H.; Preuß, H. *Theor. Chim. Acta* **1990**, *77*, 123−141.
(51) (a) Eichkorn, K.; Treutler, O.; Öhm, H.; Häser, M.; Ahlrichs, R. *Chem. Phys. Lett.* **1995**, *240*, 283−290. (b) Eichkorn, K.; Treutler, O.; Öhm, H.; Häser, M.; Ahlrichs, R. *Chem. Phys. Lett.* **1995**, *242*, 652−660. (c) Eichkorn, K.; Weigend, F.; Treutler, O.; Ahlrichs, R. *Theor. Chem. Acc.* **1997**, *97*, 119−124.
(52) These weak modes arise from hindered rotations or very flexible bending modes. The usual harmonic approximation is not valid in these cases. Moreover, an error of only a few wavenumbers results in a very large error in the vibrational partition function for these low modes and consequently in a large error in ΔG. Note, however, that the contribution of these weak modes to the ZPE is negligible, and the approximation is only necessary for the entropy.
(53) Frisch, M. J.; Trucks, G. W.; Schlegel, H. B.; Scuseria, G. E.; Robb, M. A.; Cheeseman, J. R.; Scalmani, G.; Barone, V.; Mennucci, B.; Petersson, G. A.; Nakatsuji, H.; Caricato, M.; Li, X.; Hratchian, H. P.; Izmaylov, A. F.; Bloino, J.; Zheng, G.; Sonnenberg, J. L.; Hada, M.; Ehara, M.; Toyota, K.; Fukuda, R.; Hasegawa, J.; Ishida, M.; Nakajima, T.; Honda, Y.; Kitao, O.; Nakai, H.; Vreven, T.; Montgomery, J. A., Jr.; Peralta, J. E.; Ogliaro, F.; Bearpark, M.; Heyd, J. J.; Brothers, E.; Kudin, K. N.; Staroverov, V. N.; Keith, T.; Kobayashi, R.; Normand, J.; Raghavachari, K.; Rendell, A.; Burant, J. C.; Iyengar, S. S.; Tomasi, J.; Cossi, M.; Rega, N.; Millam, J. M.; Klene, M.; Knox, J. E.; Cross, J. B.; Bakken, V.; Adamo, C.; Jaramillo, J.; Gomperts, R.; Stratmann, R. E.; Yazyev, O.; Austin, A. J.; Cammi, R.; Pomelli, C.; Ochterski, J. W.; Martin, R. L.; Morokuma, K.; Zakrzewski, V. G.; Voth, G. A.; Salvador, P.; Dannenberg, J. J.; Dapprich, S.; Daniels, A. D.; Farkas, O.; Foresman, J. B.; Ortiz, J. V.; Cioslowski, J.; Fox, D. J. *Gaussian 09*, revision B.01; Gaussian, Inc.: Wallingford, CT, 2010.
(54) Bhanage, B. M.; Divekar, S. S.; Deshpande, R. M.; Chaudhari, R. V. *J. Mol. Catal. A: Chem.* **1997**, *115*, 247−257.